

Dense and Warm Molecular Gas between Double Nuclei of the Luminous Infrared Galaxy NGC 6240

Kouichiro NAKANISHI, and Sachiko K. OKUMURA

Nobeyama Radio Observatory, Minamimaki, Minamisaku, Nagano 384-1305

nakanisi@nro.nao.ac.jp, sokumura@nro.nao.ac.jp

Kotaro KOHNO

Institute of Astronomy, The University of Tokyo, 2-21-1 Osawa, Mitaka, Tokyo 181-0015

kkohno@ioa.s.u-tokyo.ac.jp

Ryohei KAWABE

National Astronomical Observatory of Japan, 2-21-1 Osawa, Mitaka, Tokyo 181-8588

kawabe@nro.nao.ac.jp

and

Takao NAKAGAWA

Institute of Space and Astronautical Science, Japan Aerospace Exploration Agency (JAXA),

3-1-1 Yoshino-dai, Sagami-hara, Kanagawa 229-8510

nakagawa@ir.isas.jaxa.jp

(Received 2004 December 13; accepted 2005 June 6)

Abstract

High spatial resolution observations of the $^{12}\text{CO}(1-0)$, $\text{HCN}(1-0)$, $\text{HCO}^+(1-0)$, and $^{13}\text{CO}(1-0)$ molecular lines toward the luminous infrared merger NGC 6240 have been performed using the Nobeyama Millimeter Array and the RAINBOW Interferometer. All of the observed molecular emission lines are concentrated in the region between the double nuclei of the galaxy. However, the distributions of both HCN and HCO^+ emissions are more compact compared with that of ^{12}CO , and they are not coincident with the star-forming regions. The $\text{HCN}/^{12}\text{CO}$ line intensity ratio is 0.25; this suggests that most of the molecular gas between the double nuclei is dense. A comparison of the observed high $\text{HCN}/^{13}\text{CO}$ intensity ratio, 5.9, with large velocity gradient calculations suggests that the molecular gas is dense [$n(\text{H}_2) = 10^{4-6} \text{ cm}^{-3}$] and warm ($T_{\text{kin}} > 50 \text{ K}$). The observed structure in NGC 6240 may be explained by time evolution of the molecular gas and star formation, which was induced by an almost head-on collision or very close encounter of the two galactic nuclei accompanied with the dense gas and star-forming regions.

Key words: galaxies: individual(NGC 6240) — galaxies: ISM — infrared: galaxies — ISM: molecules — radio lines: ISM

1. Introduction

Luminous infrared galaxies (LIRGs) and ultra-luminous infrared galaxies (ULIRGs) are known to be huge molecular gas reservoirs [$M(\text{H}_2) \gtrsim 10^9 M_\odot$]. The results of $^{12}\text{CO}(1-0)$ and $(2-1)$ observations reveal that this molecular gas is usually concentrated at the center of the galaxies (e.g. Okumura et al. 1991; Bryant, Scoville 1999), and in general it forms a compact (radius $\lesssim 1$ kpc) rotating disk or ring (e.g., Downes, Solomon 1998; Sakamoto et al. 1999). The molecular gas within the disk or ring often shows large turbulent motions, and the molecular line profiles exhibit large velocity widths of up to 1000 km s^{-1} . The physical properties, namely the density and the temperature, of the molecular gas in LIRGs/ULIRGs are still being studied. Single-dish HCN(1-0) observations (Solomon et al. 1992; Gao, Solomon 2004a,2004b) revealed that most of their molecular gas is supposed to be dense [$n(\text{H}_2) > 10^4 \text{ cm}^{-3}$]. Single-dish observations of higher excitation ^{12}CO and ^{13}CO emissions suggest there is large amount of warm molecular gas (Aalto et al. 1995; Mauersberger et al. 1999; Yao et al. 2003). For the denser and warmer molecular gas tracers (e.g. HCN, ^{13}CO), however, the spatial distributions in LIRGs/ULIRGs are still unknown, although the physical properties of gas are keys to understand the activity of LIRGs/ULIRGs (starburst in the nuclear region and/or AGN). Moreover, the spatial variations of the molecular gas density and the temperature in the circumnuclear regions of LIRGs/ULIRGs are still unclear. For such studies, high angular resolution observations of molecular lines with radio interferometers are needed, but only a few observations have been performed so far (e.g. Aalto et al. 1997; Radford et al. 1991).

NGC 6240 ($\alpha = 16^{\text{h}}50^{\text{m}}27^{\text{s}}.83$, $\delta = +2^\circ 28' 58''.1$ (B1950); $D = 98$ Mpc, if we adopt $H_0 = 75 \text{ km s}^{-1} \text{ Mpc}^{-1}$; $1'' = 475 \text{ pc}$) is one of the most well-known nearby LIRGs, with an infrared luminosity of $L_{\text{IR}} \sim 6 \times 10^{11} L_\odot$ (Sanders, Mirabel 1996). This galaxy is a merger, with clearly visible disturbed morphology and tidal tails in optical images. NGC 6240 also has double nuclei detected in a wide range of wavelengths from X-rays to radio (Komossa et al. 2003; Thronson et al. 1990; Scoville et al. 2000; Tecza et al. 2000; Colbert et al. 1994). The apparent separation of the nuclei is $1''.5$ (710 pc) in the 15 GHz radio continuum map (Carral et al. 1990). Each of the nuclei are accompanied by an intense massive star-forming region (e.g. Alonso-Herrero et al. 2002), and both of them also host an AGN (Komossa et al. 2003). Interferometric $^{12}\text{CO}(1-0)$ and $(2-1)$ observations have been carried out by many groups (Okumura et al. 1991; Bryant, Scoville 1999; Tacconi et al. 1999). These observations show that about half of the molecular gas is concentrated in a rotating thick disk-like structure (~ 500 pc diameter) between the double nuclei, but the motion of the gas is highly disturbed and shows large velocity dispersions. The total mass of the molecular gas within a radius of ~ 500 pc is estimated to be $2-4 \times 10^9 M_\odot$, which constitutes about half of the dynamical mass (Tacconi et al. 1999). Intense HCN(1-0) emission has been detected with the IRAM 30 m telescope (Solomon et al. 1992). The obtained HCN/ $^{12}\text{CO}(1-0)$ intensity ratio is 0.15, which is a typical value for starburst galaxies, and

suggests the presence of large amounts of dense molecular gas.

In this paper, we present the results of interferometric observations of molecular emission lines toward the central region of NGC 6240. The main goal of this study is to reveal the location and distribution of dense gas and to constrain the physical properties of the molecular gas. We describe the observational parameters and data-reduction procedures in section 2, and the observational results of the ^{12}CO , HCN, HCO^+ , and ^{13}CO emission lines and continuum emission in section 3. In this section, we also refer to the observed molecular line intensity ratios and those characteristics. With these data, the physical properties of the molecular gas are discussed in section 4, and the evolutionary scenario of molecular gas and star formation according to the merging process is described in section 5. Finally, we summarize our study in section 6.

2. Observations and Data Reduction

Aperture synthesis observations toward NGC 6240 were carried out with the Nobeyama Millimeter Array (NMA) and the RAINBOW Interferometer at the Nobeyama Radio Observatory (NRO) between 1995 November – 1996 March, and 2000 January – 2003 April. The NMA consists of six 10 m-antennas equipped with cooled DSB SIS receivers. The RAINBOW Interferometer is a 7-element array combining the NMA with the NRO 45 m telescope, providing higher spatial resolution and sensitivity than those of the NMA.

We observed NGC 6240 in the following emission lines: $^{12}\text{CO}(1-0)$, $\text{HCN}(1-0)$, $\text{HCO}^+(1-0)$, and $^{13}\text{CO}(1-0)$. Except for the ^{12}CO observations, the backend we used was the Ultra-Wide-Band Correlator (UWBC; Okumura et al. 2000). For the ^{12}CO observations, the old-FX correlator was employed (Chikada et al. 1987). The quasars B1548+015, B1656+053, and B1655+077 were used for phase and amplitude reference calibrations; 3C 279, 3C 345, and 3C 454.3 were used for bandpass calibration. Uranus, Neptune, and Mars were used as absolute flux-scale calibrations for the amplitude calibrator. The uncertainties in the absolute flux scale were estimated to be $\sim 10\%$ for each observation. The HCN and HCO^+ emissions were observed simultaneously within the same correlator passband. The uv-data were calibrated with the UVPROC-II software package developed at NRO (Tsutsumi et al. 1997), and then imaged with natural UV weighting, and CLEANed, with the NRAO AIPS package.

The detailed observational parameters are summarized in table 1.

3. Results

In this section we describe the distributions and kinematical properties of the observed emission lines and calculate the intensity ratios. Our HCO^+ and ^{13}CO interferometric observations are the first ones on NGC 6240. The observational results of continuum emission at 87 GHz and 108 GHz are also presented. Table 2 summarizes the observational results.

3.1. Properties of Emission Lines

Figure 1a shows integrated intensity map of the $^{12}\text{CO}(1-0)$ emission. (No primary beam correction has been applied to the maps presented in this paper.) The distribution of the ^{12}CO emission is more extended than the size of the synthesized beam, suggesting that it is mildly resolved. The peak of the ^{12}CO emission is located between the double nuclei defined by the 15 GHz continuum peaks (Carral et al. 1990), not on either of them. Figure 2 shows the ^{12}CO velocity channel maps, and the ^{12}CO position–velocity map sliced along the double nuclei (the position angle is 20° from north to east) is presented in figure 3. The velocity profile of the ^{12}CO line at the emission peak is presented in figure 4, together with those of the HCN, HCO^+ , and ^{13}CO emissions. These plots reveal that the velocity width of the ^{12}CO line is extremely large. The full width at half maximum is 420 km s^{-1} , and the full width at zero intensity (FWZI) is $> 600 \text{ km s}^{-1}$ [the recent interferometric observations (Bryant, Scoville 1999; Tacconi et al. 1999) show that the FWZI of ^{12}CO emission is about 900 km s^{-1}]. The observed total integrated intensity of ^{12}CO is $168.3 \text{ Jy km s}^{-1}$, which is 71% of the single dish flux obtained by the IRAM 30 m telescope (Solomon et al. 1992).¹ A slight velocity gradient along the double nuclei is seen in the position–velocity map (see figure 3). The trend of the velocity gradient is the same as that in the $^{12}\text{CO}(2-1)$ map by Tacconi et al. (1999); the redshifted velocity components are in the north-east, and the blueshifted velocity ones are in the south-west. These results are consistent with the recent $^{12}\text{CO}(1-0)$ observations by Bryant and Scoville (1999).

Figure 1b shows the HCN(1–0) integrated intensity map. The continuum emission, which was detected by averaging line-free channels with an effective bandwidth of 376 MHz, was subtracted from the visibility data before creating the HCN synthesized image. Since the HCN emission is unresolved with our $2''$ beam, it must be more spatially compact than the ^{12}CO distribution. The emission peak is located between the double nuclei, within $0''.2$ of the peak position of the $^{12}\text{CO}(1-0)$ emission. It should be noted that the HCN emission peak (and also ^{12}CO) is not coincident with the current star-forming regions traced by near-infrared (NIR) emission lines; the star-forming regions are associated with both of the double nuclei (e.g. van der Werf et al. 1993; Alonso-Herrero et al. 2002). We will focus on this issue in section 5. The detected total flux of HCN emission is $14.1 \text{ Jy km s}^{-1}$, or $\sim 70\%$ of single-dish flux obtained by Solomon, Downes, and Radford (1992). The observed flux also agrees very well with the

¹ Because of the limitation of bandwidth with the old-FX correlator, continuum subtraction before imaging could not be performed on the ^{12}CO data. In order to obtain the continuum-free ^{12}CO intensity, the continuum emission contribution is removed numerically. The way we employed is as follows. From the velocity integrated map within 767 km s^{-1} (figure 1a), we primarily obtained the total emission flux (^{12}CO + continuum) of $176.9 \text{ Jy km s}^{-1}$. A 112 GHz continuum flux of 11.2 mJy was estimated from the spectrum assuming a single power-law ($S_\nu \propto \nu^{-0.81}$) between cm-wave and mm-wave (see also figure 6). Thus the total continuum emission contribution in figure 1a is estimated to be $8.59 \text{ Jy km s}^{-1}$ ($= 11.2 \text{ mJy} \times 767 \text{ km s}^{-1}$). We then subtracted this from the primarily flux, and obtained the continuum-free and velocity- and spatially-integrated ^{12}CO line flux of $168.3 \text{ Jy km s}^{-1}$.

interferometric data by Tacconi et al. (1999). Figure 1c shows the integrated intensity map of $\text{HCO}^+(1-0)$ emission. The procedure of continuum subtraction is the same as that of the HCN data, because both lines are observed simultaneously in the same passband. This is the first detection of the HCO^+ line from NGC 6240. Like the ^{12}CO and HCN emissions, the HCO^+ emission is peaked between the double nuclei. The spatial distribution of the HCO^+ emission is also compact and resembles that of the HCN emission. No systematic velocity gradient is evident in either the HCN or the HCO^+ data-cubes. This is probably due to the fact that we have not resolved their spatial distributions. Both the HCN and HCO^+ emission-line profiles (figure 4) agree reasonably well with that of ^{12}CO emission, taking into account their noise levels (20 mJy beam $^{-1}$ per channel for ^{12}CO , and 4 mJy beam $^{-1}$ for HCN and HCO^+).

An integrated intensity map of $^{13}\text{CO}(1-0)$ emission is presented in figure 1d, and emission is detected at the 4.1σ level. This is the first image ever of ^{13}CO emission from NGC 6240. The continuum emission was subtracted from the visibility data before creating the synthesized image. The flux of the ^{13}CO emission is much smaller than those of ^{12}CO and HCN. The obtained total flux is about 60% of the single dish flux obtained by Casoli, Dupraz, and Combes (1992). The synthesized beam size of the ^{13}CO map ($4''.6 \times 3''.5$) is larger than those of ^{12}CO and HCN, and the emission does not seem to be resolved. The peak of ^{13}CO also coincides with those of ^{12}CO , HCN, and HCO^+ .

3.2. Line Intensity Ratios

In this subsection, we briefly comment on the emission line intensity ratios, in brightness temperature scale,² for the molecular gas concentration between the double nuclei. Taking into account the relatively low spatial resolution of the ^{13}CO map, the line ratio is calculated using the integrated fluxes within the region of $4''.6 \times 3''.5$ ($2.2 \text{ kpc} \times 1.7 \text{ kpc}$), which corresponds to the synthesized beam size of the ^{13}CO map. This area both contains the region between the double nuclei and the double nuclei, themselves. However, the emissions are almost concentrated between the double nuclei, and the peaks of the observed emission lines coincide with each other. Thus, the line ratios within the $4''.6 \times 3''.5$ region are representative of those between the double nuclei. The error of each ratio is calculated considering the absolute flux calibration uncertainty for each observation (10%) and the noise level of the emission line maps, except for HCO^+/HCN . For the HCO^+/HCN ratio, only the noise level of each emission line map is considered, because the HCN and HCO^+ line is observed simultaneously within the same passband of the correlator.

We obtained a high $\text{HCN}/^{12}\text{CO}$ ratio of 0.25 ± 0.04 at the region between the double nuclei. This contrasts with the total integrated intensity ratio of $\text{HCN}/^{12}\text{CO} = 0.14 \pm 0.02$,

² The relation between line flux (S) and brightness temperature (T_b) is $T_b = S \cdot \lambda^2 / 2k\Omega_B$, where λ is the observed wavelength, k is the Boltzmann constant, and Ω_B is the solid angle of the region in which the line ratio is calculated.

which agrees with the single-dish values reported by Solomon, Downes, and Radford (1992). The HCN/ ^{12}CO ratio of 0.25 is higher than the mean (≈ 0.1) for LIRGs and ULIRGs, and one of the highest value among them (Gao, Solomon 2004b). Gao and Solomon (2004a) show that a large HCN/ ^{12}CO (≥ 0.1) is likely to come from regions where most of ($\gtrsim 50\%$) molecular gas is high density [$n(\text{H}_2) > 10^4 \text{ cm}^{-3}$] based on LVG calculations.

We obtain a HCO⁺/HCN ratio of 1.5 ± 0.1 . The typical HCO⁺/HCN ratio for nearby starburst galaxies and Seyfert galaxies with nuclear starbursts is 0.3 – 2 (Nguyen-Q.-Rieu et al. 1992; Kohno et al. 2001). Therefore, the value in NGC 6240 is within the range for that of starburst galaxies, but larger than the mean value ($\lesssim 1$). The high HCO⁺/HCN ratio would be due to the existence of shocked dense gas, of which the envelope is exposed to the intense ionization flux of the supernovae (Nguyen-Q.-Rieu et al. 1992, and references therein). The HCO⁺/HCN ratio of this galaxy will be discussed in a forthcoming paper together with those in the other LIRGs and mergers.

The $^{12}\text{CO}/^{13}\text{CO}$ ratio is 21 ± 6.2 at the region between the double nuclei ($2.2 \text{ kpc} \times 1.7 \text{ kpc}$). Aalto et al. (1995) found that the mean $^{12}\text{CO}/^{13}\text{CO}$ ratio is ~ 12 in their survey of infrared-bright galaxies. The ratio in NGC 6240 is thus significantly larger than the mean for starburst galaxies. Some galaxies (e.g., NGC 1614, IC 694) show a high ratio of $^{12}\text{CO}/^{13}\text{CO} > 20$, and Aalto et al. (1995) suggested that such a high ratio could be reproduced by warm turbulent molecular gas ($T > 100 \text{ K}$). They also maintain that a high $^{12}\text{CO}/^{13}\text{CO}$ ratio also implies that the optical depth of $^{12}\text{CO}(1-0)$ must be moderate [$\tau(^{12}\text{CO}) \sim 1$] and that of $^{13}\text{CO}(1-0)$ is very small [$\tau(^{13}\text{CO}) \ll 1$].

3.3. Properties of the Continuum Emission

Figure 5 shows both the 87 GHz (3.5 mm) and 108 GHz (2.8 mm) continuum images obtained using the line-free channels of the visibility data in HCN/HCO⁺ and ^{13}CO observations, respectively. Unlike the molecular lines, the continuum emission peak is almost located at the southern nucleus. Since the HCN and HCO⁺ maps and 87 GHz continuum map were created from identical uv-data, the difference between the peak positions is real. In the 87 GHz continuum map, the emission extends more than the size of the synthesized beam ($3''.6 \times 2''.2$, which corresponds to $1.7 \text{ kpc} \times 1.0 \text{ kpc}$).

Figure 6 shows the spectrum of NGC 6240 in the region surrounding the double nuclei (within $10''.8 \times 13''.6$, which corresponds to $5.1 \text{ kpc} \times 6.5 \text{ kpc}$). The total continuum flux densities at 87 GHz and 108 GHz are 16.6 mJy and 10.8 mJy, respectively. These values can be reproduced well by assuming a single power-law spectrum ($S_\nu \propto \nu^\alpha$) interpolated between the cm-wave continuum emission (Colbert et al. 1994) and 1.3 mm (228 GHz) emission (Tacconi et al. 1999). The best-fit spectral index is $\alpha = -0.81$, which is within the range of the spectral indices in both synchrotron radiation from AGN and that from supernova remnants (SNRs) (e.g., Maslowski et al. 1984; Condon 1992). Therefore, most of our observed mm-wave continuum

emission can be explained by synchrotron radiation from an AGN, SNRs, or both, come mostly from the bright southern nuclei, but there are surely some contributions from the northern nucleus. This conclusion supports the discussion by Tacconi et al. (1999).

Thermal free–free emission from star-forming regions are also expected to contribute some degree to the mm-wave continuum emission. Based on Condon (1992) and Kennicutt (1998), the relation of the thermal free–free continuum flux ($S_{\text{free–free}}$) and far-infrared luminosity (L_{FIR}) is expressed as follows:

$$\frac{S_{\text{free–free}}}{\text{mJy}} = 2.28 \times 10^{-7} \times \left(\frac{D}{\text{Mpc}}\right)^{-2} \times \left(\frac{T_e}{10^4\text{K}}\right)^{0.59} \times \left(\frac{\nu}{\text{GHz}}\right)^{-0.1} \times \frac{L_{\text{FIR}}}{L_{\odot}}, \quad (1)$$

where T_e is the electron temperature. Even if we assume all of the FIR luminosity from NGC 6240, $L_{\text{FIR}} = 4.9 \times 10^{11} L_{\odot}$ (Sanders et al. 1991), comes from the nuclear region, then the estimated free–free emission flux from H II regions at $T_e = 10^4$ K is at most ~ 7 mJy at 100 GHz. This flux value is smaller than the observed flux at 87 GHz and 108 GHz. Moreover, as can be seen in figure 6, the spectral index between 100 GHz and 228 GHz is significantly smaller than -0.1 , which is a typical index for optically thin radio free–free emission. Therefore, the free-free emission contribution on the 100 GHz continuum flux must be less than 7 mJy.

4. Dense and Warm Molecular Gas between the Double Nuclei of NGC 6240

Intensity ratios between molecular emission lines are powerful tools to probe the physical properties of molecular gas. In this section we compare the observed HCN/ ^{13}CO intensity ratio with radiative transfer model calculations, to try to constrain the physical properties of the molecular gas between the double nuclei of NGC 6240.

We have compared the observed HCN/ ^{13}CO ratio with the outcome of radiative transfer model calculations performed by Matsushita et al. (1998) based on the large velocity gradient (LVG) approximation (Goldreich, Kwan 1974; Scoville, Solomon 1974). The intense emission of the HCN line and high HCN/ ^{12}CO ratio (0.25) imply that most of the molecular gas is dense between the double nuclei (Solomon et al. 1992; Gao, Solomon 2004a). HCN emission traces molecular gas at high density [$n(\text{H}_2) > 10^4 \text{ cm}^{-3}$], and ^{13}CO emission is more excited at higher density gas than ^{12}CO due to its low optical depth. Thus, the HCN/ ^{13}CO ratio reflects the physical properties of dense molecular gas better than HCN/ ^{12}CO ratio (Matsushita et al. 1998).

Figure 7 shows the contour maps of the intensity ratio, HCN/ ^{13}CO , as a function of $Z(^{13}\text{CO})/(dv/dr)$ and $n(\text{H}_2)$, where $Z(^{13}\text{CO})$ is the fractional abundance of ^{13}CO to H_2 and dv/dr is the velocity gradient in $\text{km s}^{-1} \text{ pc}^{-1}$. The kinetic temperature (T_{kin}) in each map is shown in the top-right corner. In the LVG calculation, the single-component model was employed, and a constant relative abundance of $[^{13}\text{CO}]/[\text{HCN}] = 50$ was adopted (Solomon et al. 1979; Irvine et al. 1987). The full description of the LVG calculation is presented in Matsushita et al. (1998).

As can be seen in figure 7, the observed high ratio, $\text{HCN}/^{13}\text{CO} = 5.9 \pm 1.7$, can be reproduced in dense and warm molecular clouds. In the upper two panels showing kinetic temperatures higher than 50 K, the ratio can only be reproduced by dense gas conditions, $n(\text{H}_2) > 10^4 \text{ cm}^{-3}$. The optical depth of ^{13}CO emission under the dense and warm conditions is very small (0.01 – 0.1) in the panels of $T_{\text{kin}} = 60 \text{ K}$ and 100 K , as suggested by Aalto et al. (1995).

To explain the high $\text{HCN}/^{13}\text{CO}$ ratio under a lower gas kinetic temperature ($T_{\text{kin}} \leq 40 \text{ K}$), extremely small values of $Z(^{13}\text{CO})/(dv/dr)$ [$< 10^{-8} (\text{km s}^{-1} \text{ pc}^{-1})^{-1}$] would be required. This would happen if the velocity gradient is extremely large ($dv/dr > 10^2 \text{ km s}^{-1} \text{ pc}^{-1}$), or the ^{13}CO abundance is very low [$Z(^{13}\text{CO}) < 10^{-8}$].

If a ^{13}CO abundance of $Z(^{13}\text{CO}) = 1 \times 10^{-6}$ (Solomon et al. 1979) is adopted, a velocity gradient of $dv/dr > 10^2 \text{ km s}^{-1} \text{ pc}^{-1}$ is needed to meet the extremely small $Z(^{13}\text{CO})/(dv/dr)$ value. As we show now, this velocity gradient is, however, too large and unrealistic. We made a simple estimate of the velocity gradient from the ^{12}CO emission data. Tacconi et al. (1999) reported that, at the peak of $^{12}\text{CO}(2-1)$ emission, the line width at zero intensity (FWZI) is about 1000 km s^{-1} in a $0''.7 \times 0''.5$ ($= 330 \text{ pc} \times 240 \text{ pc}$) beam. Assuming that the ^{12}CO emission originated from a single molecular clump having the same size as the observed beam, the velocity gradient is nominally estimated to be $dv/dr \sim 3 \text{ km s}^{-1} \text{ pc}^{-1}$. Even if the size of molecular clump were 50 pc (typical for Galactic giant molecular clouds), the estimated velocity gradient would be $dv/dr \sim 18 \text{ km s}^{-1} \text{ pc}^{-1}$, which is still quite smaller than the value above. Therefore, the extremely large velocity gradient as $dv/dr > 10^2 \text{ km s}^{-1} \text{ pc}^{-1}$ is not realistic.

We now discuss the possibility that the ^{13}CO abundance is quite low. In the calculations for figure 7, a constant relative abundance of $[^{13}\text{CO}]/[\text{HCN}] = 50$ was used. The $\text{HCN}/^{13}\text{CO}$ ratio hardly depends on the HCN abundance [$Z(\text{HCN})/(dv/dr)$] because of the large optical depth of HCN (see figure 6 of Matsushita et al. 1998). On the other hand, a low ^{13}CO abundance can reproduce high $\text{HCN}/^{13}\text{CO}$ ratios. The “standard abundance” $Z(^{13}\text{CO}) = 1 \times 10^{-6}$ is obtained based on observations of molecular clouds in the inner Galaxy (Solomon et al. 1979). Although the ^{13}CO abundance at the centers of other galaxies are still not very well constrained, there appears to be little difference between the Galaxy and others (e.g. Henkel et al. 1993, 1994, 1998). The galaxy–galaxy merging may cause a low ^{13}CO abundance in the galactic center. The molecular gas in the disk of merging progenitors are predicted to converge into the centers of each of the original galaxies (Barnes, Hernquist 1996; Mihos, Hernquist 1996). In the Galaxy, the $^{12}\text{C}/^{13}\text{C}$ abundance ratio becomes larger toward the outer disk than in the Galactic center, but the difference is only a factor of $2 \sim 5$ (Wilson, Rood 1994, and references therein; Savage et al. 2002). The $^{12}\text{CO}/^{13}\text{CO}$ abundance ratio will not largely differ from that of the $^{12}\text{C}/^{13}\text{C}$ (e.g. Langer et al. 1984). Thus, the low ^{13}CO abundance might somewhat contribute to the high $\text{HCN}/^{13}\text{CO}$ ratio, but the extremely low ^{13}CO abundance [$Z(^{13}\text{CO}) < 10^{-8}$] cannot be realized. Selective dissociation of the ^{13}CO molecule might play a role, but the abundance of

^{13}CO is supposed to be affected little (van Dishoeck, Black 1988).

From the above considerations, it seems to be quite reasonable to conclude that the molecular gas is dense [$n(\text{H}_2) = 10^{4-6} \text{ cm}^{-3}$] and warm ($T_{\text{kin}} > 50 \text{ K}$) between the double nuclei of NGC 6240. Our results are also consistent with the fact that the analysis of the spectral energy distributions from the infrared to the sub-mm suggests a significant amount of warm ($T_{\text{dust}} \gtrsim 50 \text{ K}$) dust in NGC 6240 (Klaas et al. 1997; Lisenfeld et al. 2000). To confirm the high-temperature condition of the molecular gas positively, observations of higher excitation ^{12}CO and ^{13}CO emission should be performed. It is expected that the $^{12}\text{CO}/^{13}\text{CO}$ ratio in $J=2-1$ and $3-2$ show values smaller than that of $J=1-0$ (cf. Aalto et al. 1995; Hüttemeister & Aalto 2001).

Here, we make a brief comparison of physical properties of molecular gas with those of other starburst galaxies. The observational results of higher excitation ^{12}CO emission lines ($J=7-6/6-5$) combined with LVG calculations suggest that, for the central region ($r \lesssim 300 \text{ pc}$), the physical properties of molecular gas is $n(\text{H}_2) \gtrsim 10^4 \text{ cm}^{-3}$ and $T_{\text{kin}} \gtrsim 100 \text{ K}$ in NGC 253 (Bradford et al. 2003) and M 82 (Mao et al. 2000; Ward et al. 2003). Aalto et al. (1997) obtained interferometric maps of ^{12}CO , ^{13}CO , and HCN ($1-0$) toward the LIRG merger Arp 299 (IC 694+NGC 3690) in $2''3 - 5''4$ ($460 - 1090 \text{ pc}$) resolutions. At the nucleus of IC 694, the ratio $^{12}\text{CO}/^{13}\text{CO}$ is 60, the ratio HCN/ ^{12}CO is 0.11, and the ratio HCN/ ^{13}CO is 6.7. These ratios are similar to those of NGC 6240. Single-dish $^{13}\text{CO}(2-1)$ observations toward IC 694 have also been performed by Aalto et al. (1995); they concluded that the molecular gas consists of a dense [$n(\text{H}_2) = 10^{4-5} \text{ cm}^{-3}$] and warm ($T_{\text{kin}} > 50 \text{ K}$) medium based on a high $^{13}\text{CO}(2-1)/(1-0)$ ratio ($\gtrsim 2$). These previous results imply that the estimated properties of the molecular gas in NGC 6240 are common for starburst and merging galaxies.

5. Discussion

5.1. Dense Molecular Gas and Star Forming Regions

As we have shown in previous sections, NGC 6240 has a large amount of dense and warm molecular gas in the central region. The dense molecular gas distribution, however, does not coincide with that of the massive star-forming regions.

Figure 8 shows our HCN map superimposed on the distribution of NIR [Fe II] (left panel) and H_2 (right panel) emissions. The figure clearly shows that the HCN peak agrees well with the H_2 peak rather than the [Fe II] peak. The [Fe II] emission is supposed to be generated in fast shocks from supernova remnants (van der Werf et al. 1993; Sugai et al. 1997), and is thus supposed to follow the current massive star forming regions. On the other hand, the H_2 emission arise from hot molecular hydrogen excited by large-scale shock rather than UV fluorescence or X-ray heating (Sugai et al. 1997; Ohya et al. 2003). The dense gas traced by the HCN and HCO^+ emissions are concentrated between the double nuclei (see also figure 1),

whereas the massive star-forming regions traced by NIR [Fe II], Pa α , and Br γ emission lines are associated with both of the nuclei (van der Werf et al. 1993; Alonso-Herrero et al. 2002; Tecza et al. 2000). Usually the dense molecular gas is located at current massive star-forming regions in the central region of starburst galaxies and Seyferts (Kohno et al. 1999; Shibatsuka 2004). This is in contrast with what we have observed in NGC 6240. We provide a possible illustration to explain this discrepancy in the next subsection.

5.2. *Merging Evolution of Dense Molecular Gas and Star Formation in NGC 6240*

Here, we propose a possible scenario to explain the evolution of the molecular gas and star formation in NGC 6240. The origin of the unusual discrepancy between the dense gas distribution and the star-forming regions is also illustrated within it. This scenario is based on our observational results together with those of others and results from numerical simulations of galaxy–galaxy merging. A brief summary of the scenario is as follows: 1) during a galaxy–galaxy interaction, dense molecular gas is formed and intense star formation occurs in the circumnuclear regions of each of the merger progenitor galaxies, 2) an almost head-on collision or very close encounter of the nuclei cause the merging of the two dense gas concentrations, 3) the star-forming nuclei can still remain separate while the single dense gas concentration is left behind between them (this is the present view of NGC 6240), 4) a new and intense star formation will begin at some period in the dense molecular gas concentration.

We describe this scenario in more detail following the order of events.

5.2.1. *Pre-collision phase: gas accumulation and circumnuclear star formation on each merger progenitor*

At the early merging stages, the molecular gas pre-existing in the merger progenitor galaxies accumulate toward their respective galactic centers approaching each other. The gas accumulation probably results in the formation of dense molecular gas and nuclear starburst detected by the NIR observations (e.g. van der Werf et al. 1993). N-body simulations of galaxy–galaxy merging show that gas inflow, driven by gravitational torques, will cause condensations of gas clouds around the nuclei of both original galaxies (Barnes, Hernquist 1996; Mihos, Hernquist 1996; Barnes 2002). Numerical simulations also predict that the gas accumulation in each of the nuclei probably lead to considerable amount of dense molecular gas formation, which is able to cause star-formation activities within it. For example, in the merging galaxy Arp 299, most of the molecular gas is concentrated toward the nuclei (Aalto et al. 1997), and the nuclei harbor intense star formation activity (Alonso-Herrero et al. 2000).

5.2.2. *Head-on collision and formation of single dense gas concentration*

In the course of the merging process, the progenitor nuclei accompanied by dense gas concentration may suffer a nearly head-on collision or very close encounter. In the case that the impact parameter was smaller than the gas concentrations (< 1 kpc), although the nuclei and

associated stellar systems can remain gravitationally bounded, the dense molecular gas would be stripped off from the nuclei and form a single molecular gas condensation (e.g. Braine et al. 2004; Struck 1997). These events ultimately lead the nuclei to be deficient in dense molecular gas, while almost terminating the nuclear star formation.

We apply this to NGC 6240, and try to make a rough estimate of the time-scale of the collision/encounter using the relative velocity and distance between the double nuclei. The projected relative velocity is measured to be $\sim 50 \text{ km s}^{-1}$ from the stellar absorption and $\sim 150 \text{ km s}^{-1}$ from the Br γ emission (Tecza et al. 2000); thus, the actual relative velocity is assumed to be on the order of 100 km s^{-1} . From the 15 GHz continuum image (Carral et al. 1990), the projected distance of the double nuclei is 710 pc. If our viewing angle is 45° , then the actual separation of the nuclei is about 1 kpc. If we adopt 100 km s^{-1} for the relative velocity and 1 kpc for the distance, it takes about 10^7 yr for the double nuclei to move from the pericenter to the present positions. Tecza et al. (2000) estimated that the actual orbital velocity and separation between the double nuclei are 155 km s^{-1} and 1.4 kpc, respectively. They are very close to our assumed values. This time-scale is consistent with the age of the nuclear star formation. The latest star-formation activity is estimated to be suspended for $1\text{--}1.5 \times 10^7 \text{ yr}$ ago from the results of the stellar population synthesis based on the optical and NIR spectroscopic observations (Schmitt et al. 1996; Tecza et al. 2000).

5.2.3. *Post-collision phase: present view of NGC 6240*

After collision/encounter, the double nuclei leave each other from the pericenter, and the dense molecular gas concentration remains between the double nuclei. Some recently formed massive stars exist around the nuclei, but the major part of nuclear star-formation activities have already faded out because of the deficiency of dense molecular gas. This is the present view of NGC 6240.

The molecular gas concentration shows a velocity gradient within it; the north side is redshifted with respect to the south (see figure 3). This is consistent with the orbital motions of the double nuclei (Tecza et al. 2000). Tacconi et al. (1999) concluded that the velocity gradient originates from the rotational motion of the gas concentration. In a perfect head-on collision, the merged gas is expected to have no systematic velocity structure. But, in the case of an offset head-on collision or a very close encounter, the orbital angular momentum of dense gas in the pre-collision phase will remain as the rotational motion of the merged gas concentration. In our scenario, the observed velocity gradient can be explained as such rotational motion.

The molecular gas between the double nuclei is not only dense, but also warm. There is no sign of intense massive star formation or prominent AGN activity between the double nuclei, and thus ultraviolet radiation from them should not be a principal heating source. One probable heating source is dynamical energy sources, that is to say, turbulence and shocks. The large velocity width of the molecular emission lines and complicated distributions of molecular

gas imply the existence of large turbulence within the dense gas concentrations (Tacconi et al. 1999). Extraordinary bright shock excited NIR H₂ emission has been detected in this object (Sugai et al. 1997; Ohyama et al. 2000; Gerssen et al. 2004), and the H₂ peak agrees well with that of the dense gas concentration (see figure 8). These facts imply that the large turbulence and the intense shocks causes a high molecular gas temperature.

5.2.4. *New starburst in dense gas concentration*

A brand-new starburst will begin in the dense gas concentration in the near future. Tacconi et al. (1999) estimated the dissipation time-scale for random velocities within the gas concentration to be $\leq 10^7$ yr, and suggest that NGC 6240 may experience the next major starburst within the gas concentration. Some external effects on the dense gas might also proceed star-formation. The “starburst driven starburst” proposed by Taniguchi, Trentham, and Shioya (1998) is one of the possible mechanisms. Dense gas clumps can collapse under high external pressure caused by the starburst driven super-wind from the double nuclei (Ohyama et al. 2003), and massive star-formation will be induced in them.

Star formation within the dense gas concentration may have already commenced, but it is very young ($\ll 10^7$ yr) and suffering from large interstellar absorption because of huge amounts of interstellar medium. There exists a hint that the starburst activity should not be older than several 10^6 yr, if the starburst has already begun. There is no evident sign of strong supernova explosions, because of the weakness of cm-wave radio continuum emission and NIR [Fe II] emission between the double nuclei (Colbert et al. 1994; van der Werf et al. 1993).

Mid-infrared (MIR) spectroscopic observations with the Infrared Space Observatory (ISO) revealed that the star-forming regions in NGC 6240 suffer from large interstellar extinction. The extinction toward the star-forming regions, estimated from the emission line flux ratio between MIR [Ne II] and NIR Br γ , is $A_V = 15 - 20$ mag (corresponding to $A_K \sim 1.5 - 2$ mag) in the simplified screen assumption (Lutz et al. 2003). This estimation is larger (10 - 15 mag in A_V) than the extinction derived from optical and NIR spectroscopic observations (Veilleux et al. 1995; Tecza et al. 2000). Therefore, the spatial distributions seen even at the NIR wavelength ([Fe II], Pa α , and Br γ emission lines) may not totally trace star-forming regions deeply obscured by the interstellar medium. Although the location of an obscured star-forming region has not been identified yet because the ISO aperture ($> 10''$) covers the whole nuclear region of NGC 6240, a young star-forming region may hide in the dense molecular gas concentration between the double nuclei.

6. Summary

We have carried out high spatial-resolution observations of molecular lines toward the infrared luminous merger NGC 6240 using the NMA and the RAINBOW interferometers. The ¹²CO emission peak lies between the double nuclei of this galaxy; our results confirm the

previous interferometric $^{12}\text{CO}(1-0/2-1)$ observations. Our new high-resolution HCN and HCO^+ observations reveal that the emissions are also peaked between the double nuclei, and are not spatially resolved with our beam size of $2''$. The ratio $\text{HCN}/^{12}\text{CO}$ is as high as 0.25 in the region between the double nuclei. The ^{13}CO emission has also been observed, and it turns out to be much weaker than others.

The comparison between the high ratio $\text{HCN}/^{13}\text{CO} = 5.9$ and the LVG calculations suggests that the molecular gas is substantially dense and warm. The estimated molecular hydrogen density and kinetic temperature are $n(\text{H}_2) = 10^{4-6} \text{ cm}^{-3}$ and $T_{\text{kin}} > 50 \text{ K}$, respectively. These physical properties are similar to those seen at the centers of the nearby starburst galaxies and infrared luminous mergers.

The observed characteristics that most of the dense and warm gas in NGC 6240 is located between the starburst nuclei is very unusual among the infrared luminous mergers observed so far. We propose a scenario to explain the evolution of dense molecular gas and starbursts, and to resolve the discrepancy between their locations in NGC 6240. In our scenario, a head-on collision or very close encounter of the star-forming nuclei caused the merging of dense molecular gas associated with both nuclei. At the present moment, the double star-forming nuclei are still apart from each other, but a dense and warm molecular gas concentration has been left between them. In the near future, a new starburst is expected to commence within the dense gas concentration.

The authors wish to express their deep gratitude to Dr. Satoki Matsushita for kindly providing us with his LVG calculation results. We are grateful to Prof. Paul van der Werf for readily furnishing us with his high-quality near-infrared images of NGC 6240. We are indebted to Dr. Baltasar Vila-Vilaró for carefully reading the manuscript and valuable comments. We would like to thank Dr. Dennis Downes, the referee, for his helpful comments. We thank the NRO staff for the operation of the telescopes and assisting us in our observations. K.N. was financially supported by the Japan Society for the Promotion of Science (JSPS). K.N. was also partially supported by a Grant-in-Aid for Scientific Research from the Ministry of Education, Culture, Sports, Science and Technology (MEXT) No. 15037212. K.K. was financially supported by JSPS Grant-in-Aid for Scientific Research (B) No.14403001 and MEXT Grant-in-Aid for Scientific Research on Priority Areas No.15071202. The Nobeyama Radio Observatory is a branch of the National Astronomical Observatory of Japan, the National Institutes of Natural Sciences (NINS).

References

- Aalto, S., Booth, R. S., Black, J. H., & Johansson, L. E. B. 1995, *A&A*, 300, 369
Aalto, S., Radford, S. J. E., Scoville, N. Z., & Sargent, A. I. 1997, *ApJ*, 475, L107
Alonso-Herrero, A., Rieke, G. H., Rieke, M. J., & Scoville, N. Z. 2000, *ApJ*, 532, 845

- Alonso-Herrero, A., Rieke, G. H., Rieke, M. J., & Scoville, N. Z. 2002, *AJ*, 124, 166
- Barnes, J. E. 2002, *MNRAS*, 333, 481
- Barnes, J. E., & Hernquist, L. 1996, *ApJ*, 471, 115
- Bradford, C. M., Nikola, T., Stacey, G. J., Bolatto, A. D., Jackson, J. M., Savage, M. L., Davidson, J. A., & Higdon, S. J. 2003, *ApJ*, 586, 891
- Braine, J., Lisenfeld, U., Duc, P.-A., Brinks, E., Charmandaris, V., & Leon, S. 2004, *A&A*, 418, 419
- Bryant, P. M., & Scoville, N. Z. 1999, *AJ*, 117, 2632
- Carral, P., Turner, J. L., & Ho, P. T. P. 1990, *ApJ*, 362, 434
- Casoli, F., Dupraz, C., & Combes, F. 1992, *A&A*, 264, 55
- Chikada, Y., Ishiguro, M., Hirabayashi, H., Morimoto, M., & Morita, K.-I., 1987, *Proc. IEEE*, 75, 1203
- Colbert, E. J. M., Wilson, A. S., & Bland-Hawthorn, J. 1994, *ApJ*, 436, 89
- Condon, J. J. 1992, *ARA&A*, 30, 575
- Downes, D., & Solomon, P. M. 1998, *ApJ*, 507, 615
- Downes, D., Solomon, P. M., & Radford, S. J. E., 1993, *ApJ*, 414, L13
- Gao, Y., & Solomon, P. M. 2004a, *ApJS*, 152, 63
- Gao, Y., & Solomon, P. M. 2004b, *ApJ*, 606, 271
- Gerssen, J., van der Marel, R. P., Axon, D., Mihos, J. C., Hernquist, L., & Barnes, J. E. 2004, *AJ*, 127, 75
- Goldreich, P., & Kwan, J. 1974, *ApJ*, 189, 441
- Henkel, C., Chin, Y.-N., Mauersberger, R., & Whiteoak, J. B. 1998 *A&A*, 329, 443
- Henkel, C., Mauersberger, R., Wiklind, T., Huettmeister, S., Lemme, C., & Millar, T. J. 1993, *A&A*, 268, L17
- Henkel, C., Whiteoak, J. B., & Mauersberger, R. 1994, *A&A*, 284, 17
- Hüttemeister, S., & Aalto, S. 2001, in *ASP Conf. Ser. 249.*, *The Central Kiloparsec of Starbursts and AGN: The La Palma Connection*, ed. J. H. Knapen, J. E. Beckman, I. Shlosman, & T. J. Mahoney (San Francisco: ASP), 619
- Irvine, W. M., Goldsmith, P. F., & Hjalmarsen, A. 1987, in *Interstellar Processes*, ed. D. J. Hollenbach & H. A. Thronson, Jr. (Dordrecht: Reidel), 561
- Kennicutt, R. C., Jr. 1998, *ARA&A*, 36, 189
- Klaas, U., Haas, M., Heinrichsen, I., & Schulz, B. 1997, *A&A*, 325, L21
- Kohno, K., Kawabe, R., & Vila-Vilaró, B., 1999, *ApJ*, 511, 157
- Kohno, K., Matsushita, S., Vila-Vilaró, B., Okumura, S. K., Shibatsuka, T., Okiura, M., Ishizuki, S., & Kawabe, R. 2001, in *ASP Conf. Ser. 249.*, *The Central Kiloparsec of Starbursts and AGN: The La Palma Connection*, ed. J. H. Knapen, J. E. Beckman, I. Shlosman, & T. J. Mahoney (San Francisco: ASP), 672
- Komossa, S., Burwitz, V., Hasinger, G., Predehl, P., Kaastra, J. S., & Ikebe, Y. 2003, *ApJ*, 582, L15
- Langer, W. D., Graedel, T. E., Frerking, M. A., & Armentrout, P. B. 1984, *ApJ*, 277, 581
- Lisenfeld, U., Isaak, K. G., & Hills, R. 2000, *MNRAS*, 312, 433
- Lutz, D., Sturm, E., Genzel, R., Spoon, H. W. W., Moorwood, A. F. M., Netzer, H., & Sternberg, A. 2003, *A&A*, 409, 867

- Mao, R. Q., Henkel, C., Schulz, A., Zielinsky, M., Mauersberger, R., Störzer, H., Wilson, T. L., & Gensheimer, P. 2000, *A&A*, 358, 433
- Maslowski, J., Pauliny-Toth, I. I. K., Witzel, A., & Kuehr, H. 1984, *A&A*, 139, 85
- Matsushita, S., Kohno, K., Vila-Vilaró, B., Tosaki, T., & Kawabe, R. 1998, *ApJ*, 495, 267
- Mauersberger, R., Henkel, C., Walsh, W., & Schulz, A. 1999, *A&A*, 341, 256
- Mihos, J. C., & Hernquist, L. 1996, *ApJ*, 464, 641
- Nguyen, Q.-Rieu, Jackson, J. M., Henkel, C., Truong, B., & Mauersberger, R. 1992, *ApJ*, 399, 521
- Ohyama, Y., et al. 2000, *PASJ*, 52, 563
- Ohyama, Y., Yoshida, M., & Takata, T. 2003, *AJ*, 126, 2291
- Okumura, S. K., et al. 2000, *PASJ*, 52, 393
- Okumura, S. K., Kawabe, R., Ishiguro, M., Kasuga, T., Morita, K.-I., & Ishizuki, S. 1991, in *IAU Symp. 146, Dynamics of Galaxies and Their Molecular Cloud Distributions*, ed. F. Combes & F. Casoli (Dordrecht: Kluwer), 425
- Radford, S. J. E., et al. 1991, in *IAU Symp. 146, Dynamics of Galaxies and Their Molecular Cloud Distributions*, ed. F. Combes & F. Casoli (Dordrecht: Kluwer), 303
- Sakamoto, K., Scoville, N. Z., Yun, M. S., Crosas, M., Genzel, R., & Tacconi, L. J. 1999, *ApJ*, 514, 68
- Sanders, D. B., & Mirabel, I. F. 1996, *ARA&A*, 34, 749
- Sanders, D. B., Scoville, N. Z., & Soifer, B. T. 1991, *ApJ*, 370, 158
- Savage, C., Apponi, A. J., Ziurys, L. M., & Wyckoff, S. 2002, *ApJ*, 578, 211
- Schmitt, H. R., Bica, E., & Pastoriza, M. G. 1996, *MNRAS*, 278, 965
- Scoville, N. Z., et al. 2000, *AJ*, 119, 991
- Scoville, N. Z., & Solomon, P. M. 1974, *ApJ*, 187, L67
- Shibatsuka, T. 2004, PhD Thesis, The University of Tokyo
- Solomon, P. M., Downes, D., & Radford, S. J. E. 1992, *ApJ*, 387, L55
- Solomon, P. M., Scoville, N. Z., & Sanders, D. B. 1979, *ApJ*, 232, L89
- Struck, C. 1997, *ApJS*, 113, 269
- Sugai, H., Malkan, M. A., Ward, M. J., Davies, R. I., & McLean, I. S. 1997, *ApJ*, 481, 186
- Tacconi, L. J., Genzel, R., Tecza, M., Gallimore, J. F., Downes, D., & Scoville, N. Z. 1999, *ApJ*, 524, 732
- Taniguchi, Y., Trentham, N., & Shioya, Y. 1998, *ApJ*, 504, L79
- Tecza, M., Genzel, R., Tacconi, L. J., Anders, S., Tacconi-Garman, L. E., & Thatte, N. 2000, *ApJ*, 537, 178
- Thronson, H. A., Majewski, S., Descartes, L., & Hereld, M. 1990, *ApJ*, 364, 456
- Tsutsumi, T., Morita, K.-I., & Umeyama, S. 1997, in *ASP Conf. Ser. 125, Astronomical Data Analysis Software and Systems VI*, ed. G. Hunt & H. E. Payne (San Francisco: ASP), 50
- van der Werf, P. P., Genzel, R., Krabbe, A., Blietz, M., Lutz, D., Drapatz, S., Ward, M. J., & Forbes, D. A. 1993, *ApJ*, 405, 522
- van Dishoeck, E. F., & Black, J. H. 1988, *ApJ*, 334, 771
- Veilleux, S., Kim, D.-C., Sanders, D. B., Mazzarella, J. M., & Soifer, B. T. 1995, *ApJS*, 98, 171
- Ward, J. S., Zmuidzinas, J., Harris, A. I., & Isaak, K. G. 2003, *ApJ*, 587, 171
- Wilson, T. L., & Rood, R. 1994, *ARA&A*, 32, 191

Yao, L., Seaquist, E. R., Kuno, N., & Dunne, L. 2003, *ApJ*, 588, 771

Table 1. Observational log.

	^{12}CO	HCN	HCO^+	^{13}CO
Array configurations	AB,C,D	Rb*, AB, C	Rb, AB, C	C, D
Observed frequency (GHz)	112.52	86.52	87.06	107.57
Year of observation	1995–1996	2000–2002	2000–2002	2001–2003
Correlator	old-FX	UWBC	UWBC	UWBC
Frequency resolution (MHz)	0.3125	8	8	8
Bandwidth (MHz)	320	1024	1024	1024
Synthesized beam($''$)	2.2×2.1	2.0×1.7	2.0×1.7	4.6×3.5

* RAINBOW.

Table 2. Observational results.

	^{12}CO	HCN	HCO^+	^{13}CO
On-source integration time (hour)	9.7	17.0	17.0	27.1
Velocity resolution of data cube (km s^{-1})	21.3	55.4	55.1	178.4
Typical noise level (mJy beam^{-1})	20	4	4	2
Typical T_{sys} in SSB (K)	760	330	330	400
Half intensity size ($''$)	3.0×2.4	2.0×1.7	2.3×2.1	4.6×3.5
Line width (FWHM; km s^{-1})	420	390	420	450
Total flux (Jy km s^{-1})	168.3	14.1	20.9	3.7
NMA/IRAM 30 m flux ratio*	0.71	0.67	—	0.58
Luminosity ($\text{K km s}^{-1} \text{pc}^2$)	4.0×10^9	5.7×10^8	8.3×10^8	9.7×10^7
Ratio to ^{12}CO (total) †	—	0.14	0.21	0.024
Ratio to ^{12}CO ($<4''6 \times 3''5$) †	—	0.25	0.37	0.047
Ratio to HCN (total) †	7.1	—	1.5	0.17
Continuum flux (mJy)	—	16.6	16.6	10.8

* References for the IRAM 30m observations; ^{12}CO and HCN: Solomon et al. (1992), ^{13}CO : Casoli, Dupraz, & Combes (1992). † All ratios are in brightness temperature scale.

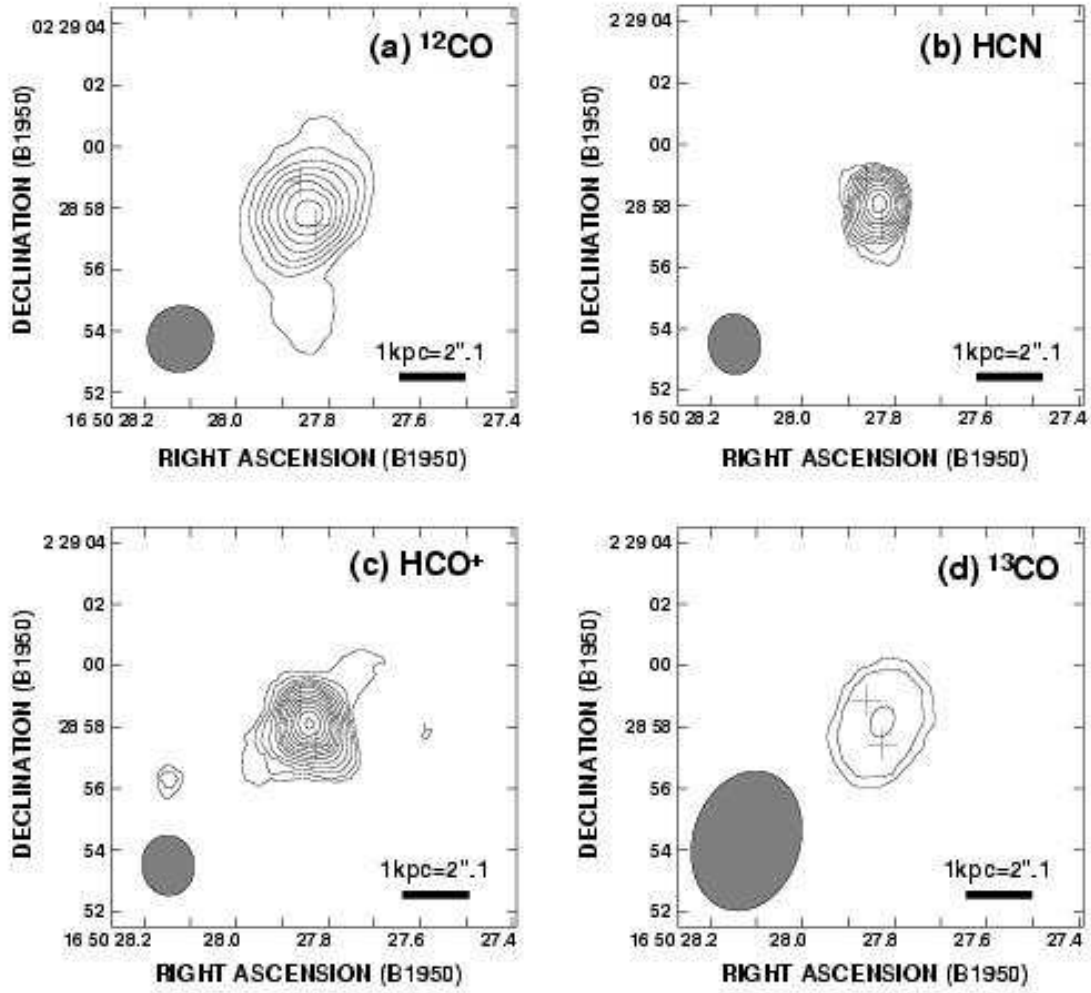


Fig. 1. Integrated intensity maps of (a) $^{12}\text{CO}(1-0)$, (b) $\text{HCN}(1-0)$, (c) $\text{HCO}^+(1-0)$, and (d) $^{13}\text{CO}(1-0)$ emission in NGC 6240. The contour levels in each map are (a) 2, 4, 6, ..., 16σ , where $1\sigma = 2.6 \text{ Jy km s}^{-1}$, (b) 2, 3, 4, ..., 11σ , where $1\sigma = 0.79 \text{ Jy km s}^{-1}$, (c) 2, 3, 4, ..., 14σ , where $1\sigma = 0.78 \text{ Jy km s}^{-1}$, and (d) 2, 3, 4, σ , where $1\sigma = 0.94 \text{ Jy km s}^{-1}$. The synthesized beam is shown at the bottom-left corner of each map. The crosses show the peak positions of 15 GHz continuum (Carral et al. 1990), which coincide with the positions of the double nuclei (AGNs). No primary beam correction has been applied.

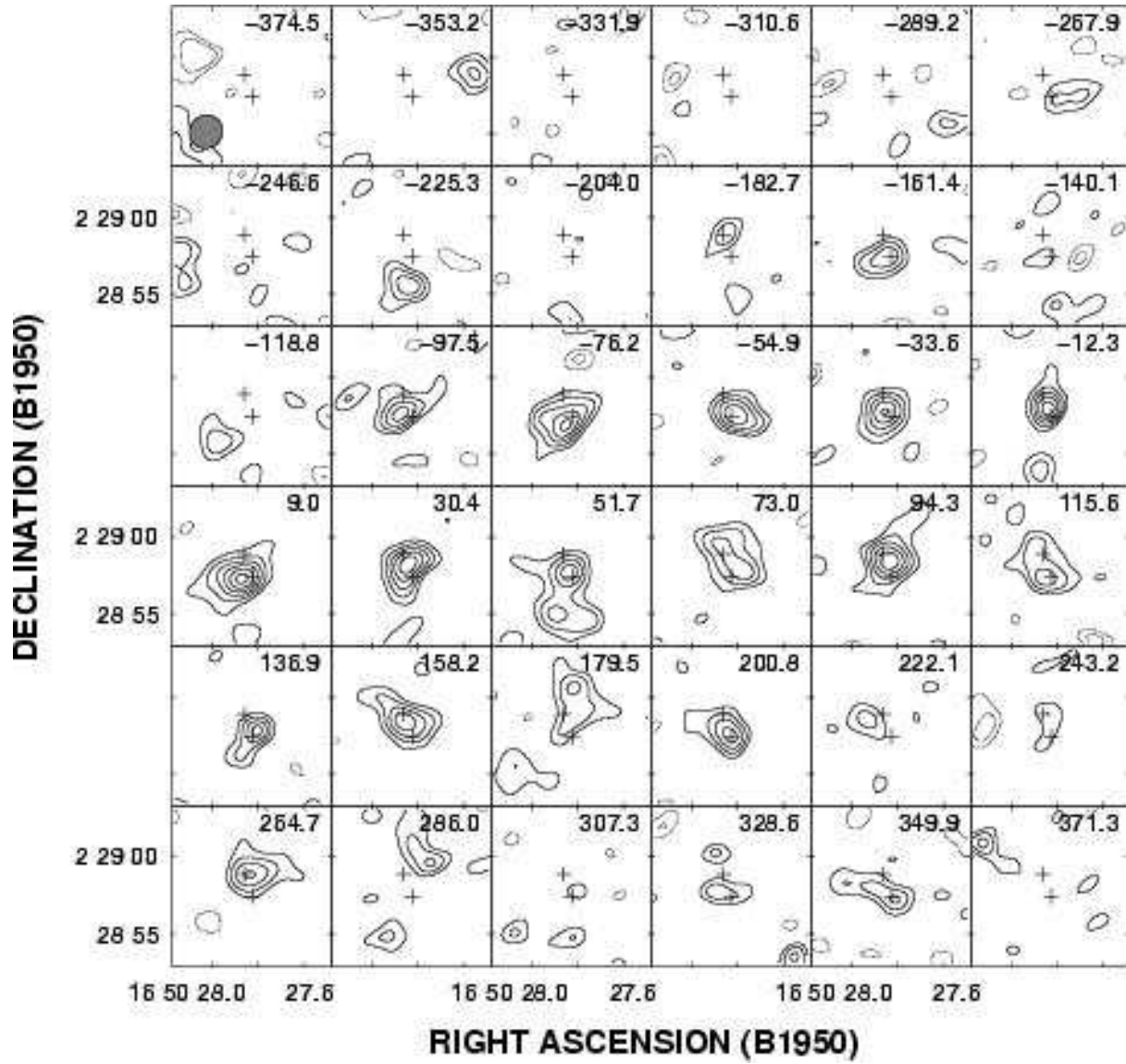


Fig. 2. Velocity channel maps of the $^{12}\text{CO}(1-0)$ emission in the central $10'' \times 10''$ ($4.8 \text{ kpc} \times 4.8 \text{ kpc}$) region of NGC 6240. The contour levels are $-3, -2, 2, 3, 4, 5, 6\sigma$, where $1\sigma = 20 \text{ mJy beam}^{-1}$ (negative contours are dashed). The labels in each channel (top right) are velocity offsets, in km s^{-1} , from the systemic velocity (v_{LSR}) of 7339 km s^{-1} (Downes et al. 1993). The velocity width of each channel is 21.3 km s^{-1} . The crosses show the peak positions of the 15 GHz continuum emissions (Carral et al. 1990).

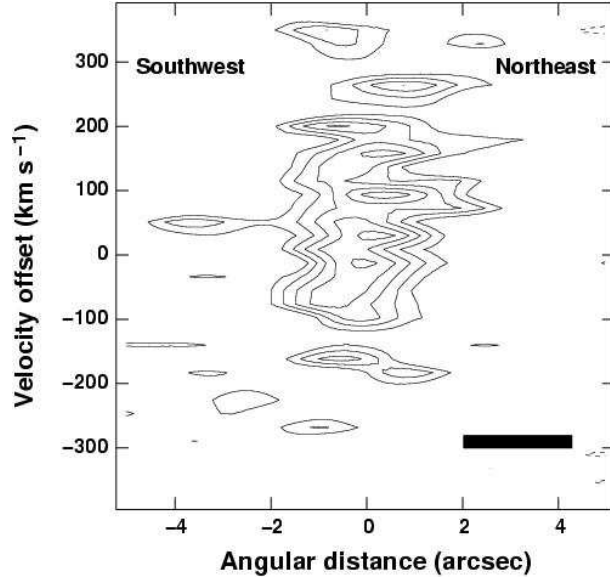


Fig. 3. Position–velocity map of $^{12}\text{CO}(1-0)$ emission from NGC 6240 along the double nuclei (position angle is 20°). The abscissa is the angular distance from the ^{12}CO emission peak ($\alpha = 16^{\text{h}}50^{\text{m}}27^{\text{s}}.85$, $\delta = +2^\circ28'57''.9$; B1950). The ordinate is the velocity offset relative to the systemic velocity of 7339 km s^{-1} . The contour levels are $-2, 2, 3, 4, 5, 6\sigma$, where $1\sigma = 20 \text{ mJy beam}^{-1}$ (negative contours are dashed). The black rectangle represents a single resolution element in both dimensions.

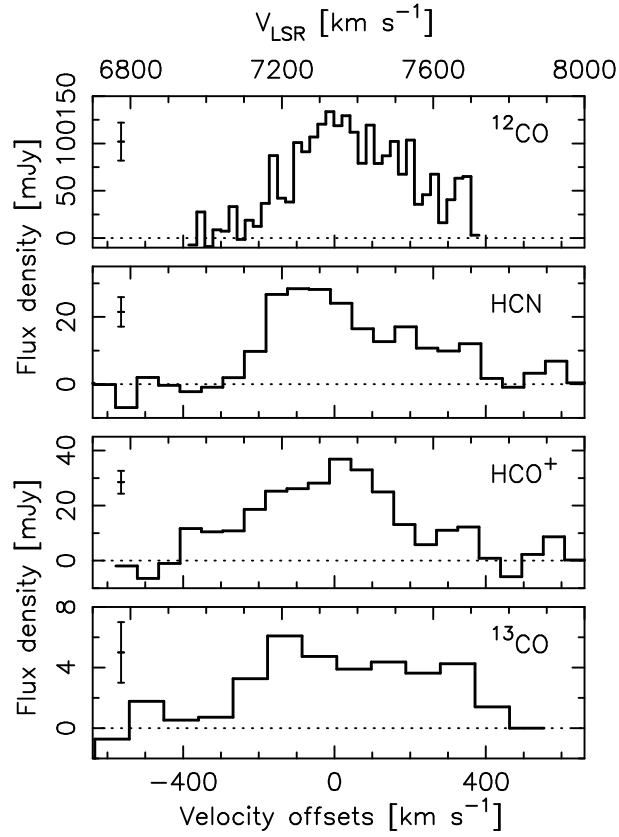


Fig. 4. Line profiles of $^{12}\text{CO}(1-0)$ (top panel), $\text{HCN}(1-0)$ (second from top), $\text{HCO}^+(1-0)$ (third from top), and $^{13}\text{CO}(1-0)$ (bottom) at the position of the $^{12}\text{CO}(1-0)$ emission peak of NGC 6240. In each panel, the abscissa is labeled with both the velocity offsets from the systemic velocity of 7339 km s^{-1} (lower side) and the LSR velocity (upper side).

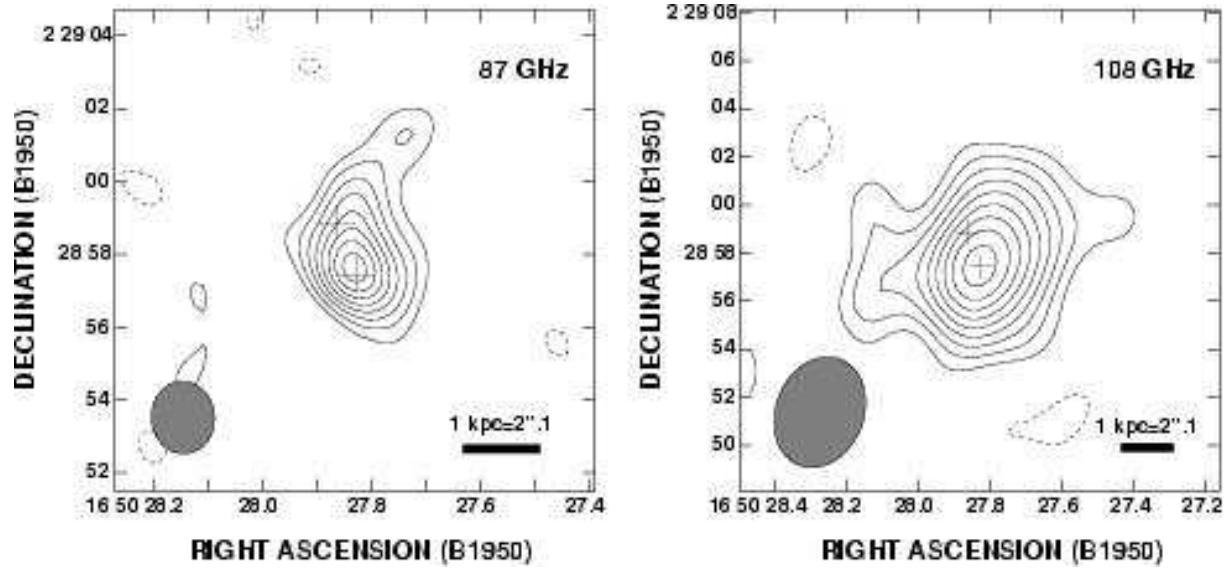


Fig. 5. Continuum maps at 87 GHz (left panel) and 108 GHz (right panel) toward the center of NGC 6240. The contour levels are $-2, 2, 3, 4, \dots, 9\sigma$, where $1\sigma = 1.0$ mJy for the 87 GHz map, and $-2, 2, 3, 4, \dots, 10\sigma$, where $1\sigma = 0.7$ mJy for the 108 GHz map (negative contours are dashed). The synthesized beam is shown at the bottom-left corner of the map. The crosses show the peak positions of the 15 GHz continuum (Carral et al. 1990). No primary beam correction has been applied.

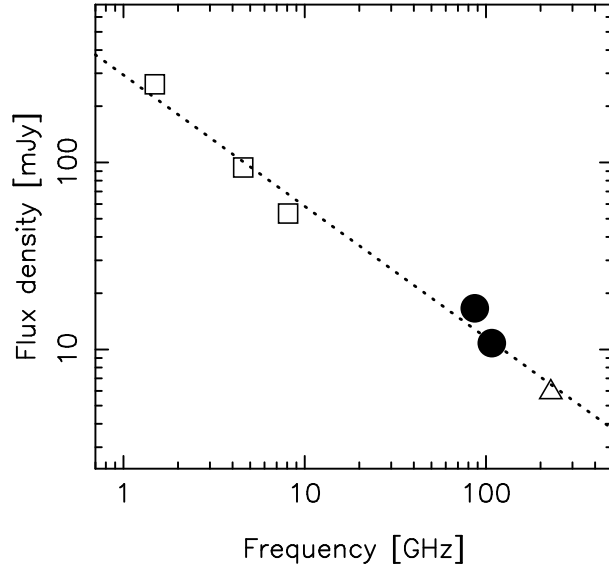


Fig. 6. The cm- to mm-wave continuum spectrum of NGC 6240 nuclear region within $10''8 \times 13''6$. Data are from Colbert et al. (1994) (open squares), Tacconi et al. (1999) (open triangle), and this work (filled circles). The errors for each data point are smaller than the sizes of the symbols in the plot. The dotted line represents the best fit power-law with an spectral index of -0.81 .

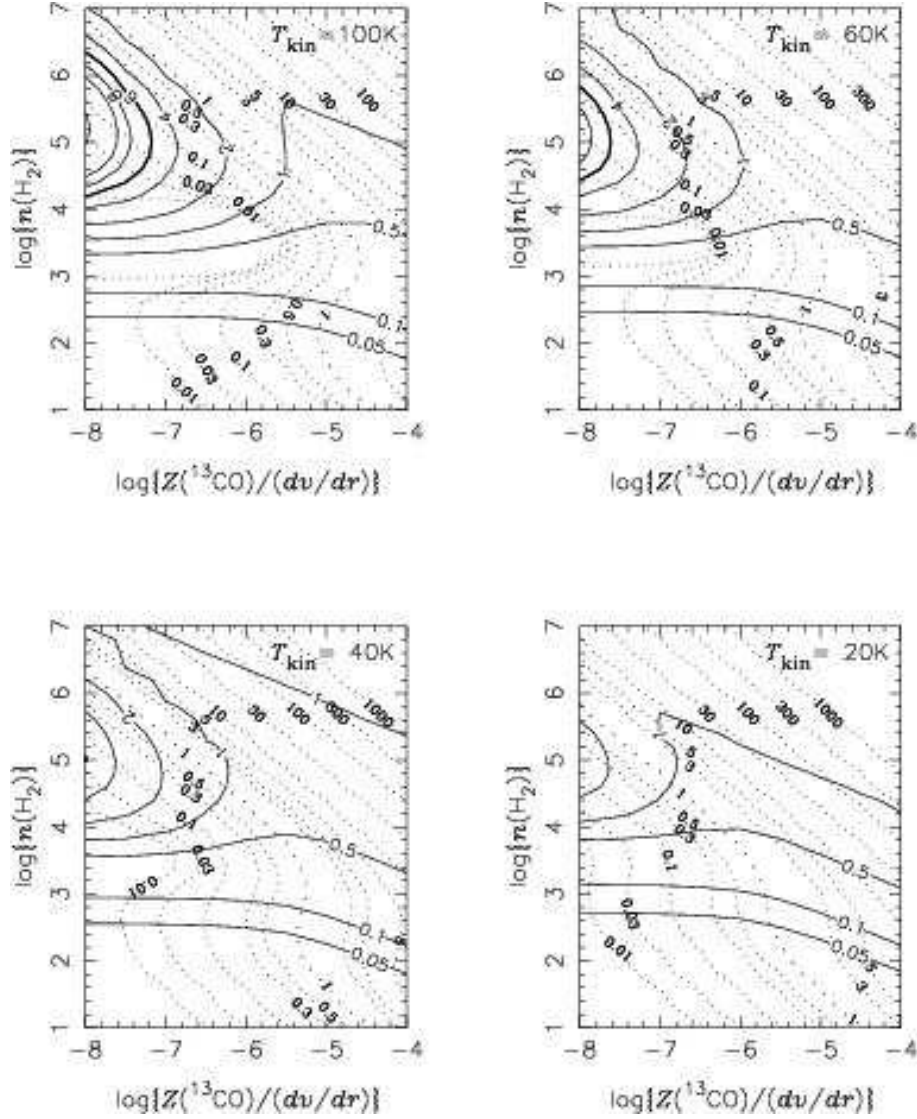


Fig. 7. Simulated HCN/ ^{13}CO intensity ratio (solid contour) and opacity of ^{13}CO emission [$\tau_{1-0}(^{13}\text{CO})$; dotted contour] obtained from LVG calculations by Matsushita et al. (1998). A fixed relative abundance of $[^{13}\text{CO}]/[\text{HCN}]=50$ is assumed. Models with kinetic temperatures (T_{kin}) of 20, 40, 60, and 100 K are presented (T_{kin} is indicated in the top right corner of each panel). The ordinate is $Z(^{13}\text{CO})/(dv/dr)$, where $Z(^{13}\text{CO})$ is the relative abundance of ^{13}CO to the H_2 and dv/dr is the velocity gradient in $\text{km s}^{-1} \text{pc}^{-1}$. The abscissa is the number density of molecular hydrogen in cm^{-3} . The contour levels in solid lines (HCN/ ^{13}CO) are 0.05, 0.1, 0.5, 1, 2, 4, 6, 8, 10, and 15. The thick solid curve indicates a HCN/ ^{13}CO ratio of 6. The contour levels in dotted lines [$\tau_{1-0}(^{13}\text{CO})$] are 0.01, 0.03, 0.1, 0.3, 0.5, 1.0, 3.0, 5.0, 10.0, 30.0, 100.0, 300.0, and 1000.0. The opacity of unity are shown as thick dotted curves.

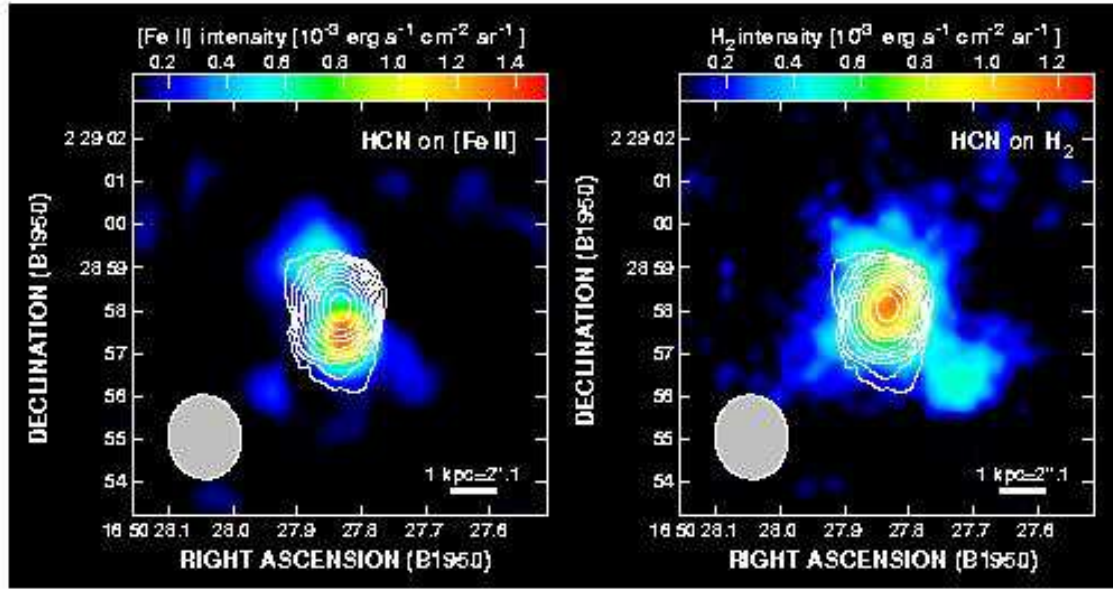


Fig. 8. HCN integrated intensity map (contours) superimposed on the near-infrared [Fe II] at $1.644 \mu\text{m}$ (left panel) and $\text{H}_2(v=1-0 S(1))$ at $2.121 \mu\text{m}$ (right panel) emission line maps from van der Werf et al.(1993, 2005 in preparation). The contour levels for HCN are the same as figure 1b. The synthesized beam of the HCN is shown at the bottom-left corner.